Biosensors and Bioelectronics 131 (2019) 280–286

Contents lists available at ScienceDirect

Biosensors and Bioelectronics

journal homepage: www.elsevier.com/locate/bios

Oscillatory flow-assisted efficient target enrichment with small volumes of sample by using a particle-based microarray device

Sanghyun Lee[a,1], Wonhyung Lee[a,1], Hojin Kim[b], Pan Kee Bae[c], Jaechan Park[d], Joonwon Kim[a,*]

[a] Department of Mechanical Engineering, Pohang University of Science and Technology (POSTECH), 77 Cheongam-Ro, Nam-Gu, Pohang, Gyeongbuk 37673, Republic of Korea
[b] BioMEMS Lab., RadianQbio, 53 Gasan Digital 2-Ro, Geumcheon-Gu, Seoul 08588, Republic of Korea
[c] BioNano Health Guard Research Center, 125 Gwahak-Ro, Yuseong-Gu, Daejeon 34141, Republic of Korea
[d] Department of Neurosurgery, School of Medicine, Kyungpook National University, 680 Gukchaebosang-Ro, Jung-Gu, Daegu 41944, Republic of Korea

ARTICLE INFO

Keywords:
Microfluidics
Microarray
Oscillatory flow
Immunoassay

ABSTRACT

In the study, we describe an oscillatory flow-assisted efficient target enrichment method by using a particle-based microarray device. Periodic oscillating flow effectively increased the mixing and binding performance between the target molecules in the sample solution and surface functionalized microparticles. Particles were trapped, secured, and released with an elastic microvalve structure operated via differences in the flow conditions. Single particle (20-μm diameter) trapping efficiency exceeded 95%. Secured particles can freely move inside each array element based on oscillating sample flow. Furthermore, the particles can be released from the array and collected at the outlet of the device, and this provides an opportunity for further off-chip analysis. As a proof-of-concept, we used the interaction between streptavidin-coated microparticles and fluorescence labeled biotin solution and demonstrated that target enrichment and detection based on oscillatory flow were significantly more efficient than that based on unidirectional or static flow. The applicability of the method was further examined by conducting an on-chip immunoassay to detect the presence of anti-Zika nonstructural protein 1 (NS1) monoclonal antibody. The limit of detection (LOD) was as low as 1 ng/mL with an assay time of only 10 min and less than 10 μL of sample consumption.

1. Introduction

With the advancement of microfluidic lab-on-a-chip (LOC) platforms, a variety of chemical and biological reactions can be performed with several advantages including cost reduction, rapid analysis, automation, and portability. With respect to the operation of LOC platforms, several microfluidic unit operating functions are required such as transportation, metering, mixing, incubation, and sorting. Among the functions, efficient mixing in microfluidic devices (typical channel dimensions of hundreds of micrometers) is one of the most critical functions to perform a variety of biochemical reactions such as cell/tissue staining and protein analysis. Low mixing efficiency and incomplete mixing significantly decrease overall assay performance.

Generally, microscale fluid mixing process is not as efficient as macroscale fluid mixing since microscale fluid mixing phenomena typically rely on molecular diffusion due to the low Reynolds number (*Re*) of the microscale flow. Reynolds number is defined as the ratio of viscous forces to inertial forces, and this is defined as $Re = \rho UL/\mu$ where ρ denotes the density of the fluid, U denotes the velocity of the flow, L denotes the characteristic linear dimension, and μ denotes the dynamic viscosity of the fluid. Owing to small channel dimensions, *Re* is typically very small in microscale flow, and this implies that the viscous forces dominate over inertial forces within the flow. Thus, flow is laminar, and it is difficult to achieve turbulent mixing. Therefore, the mixing of fluids in microfluidic devices generally constitutes a time-consuming process.

Thus, there have been many reports to enhance mixing efficiency in microscale flow (Suh and Kang, 2010; Ward and Fan, 2015). They are categorized into two major approaches, namely passive and active mixing. Passive mixing approaches utilize the geometries of a microchannel to stretch and fold fluid interfaces to improve mixing and mass transfer (Hong et al., 2004; Kim et al., 2005; Kwak et al., 2016; Li et al., 2014; Lin et al., 2013; Therriault et al., 2003). The approaches do not require any peripheral devices and external stimulus. However, they

* Corresponding author.
E-mail address: Joonwon@postech.ac.kr (J. Kim).
[1] Sanghyun Lee and Wonhyung Lee contributed equally to the study.

https://doi.org/10.1016/j.bios.2019.01.067
Received 27 November 2018; Received in revised form 21 January 2019; Accepted 27 January 2019
Available online 20 February 2019
0956-5663/

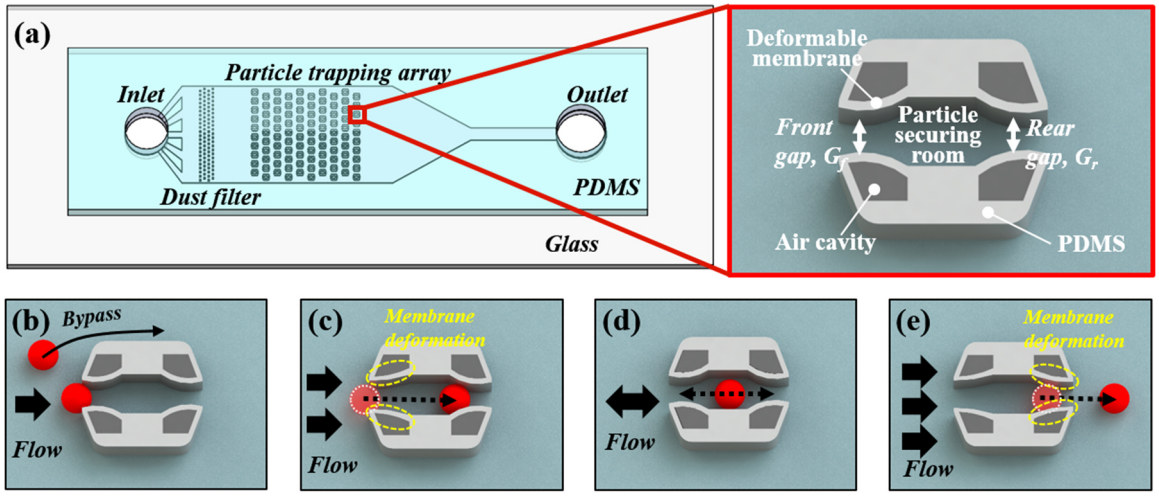

Fig. 1. Device design and working principle (a) Schematic illustration of the device. The PDMS-glass hybrid microfluidic device exhibits single-layer channel configuration. The red box shows the components of an array element. (b) Particle trapping. The introduced particle is trapped at the front gap. (c) Particle securing. The trapped particle passes through the gap by flow-induced membrane deformation. (d) Particle oscillation. The secured particle is oscillated inside the array under a proper oscillating input. (e) Particle releasing. The secured particle escapes from the array via flow-induced membrane deformation.

generally require microchannels with extremely long lengths to accomplish complete mixing. Additionally, device flexibility is limited since the degree of mixing is dependent on the channel geometry, and users cannot control the mixing process. Active approaches utilize external stimuli (e.g., mechanic, electric, acoustic, and magnetic) to agitate fluids inside the channel by using power-consuming components (Ahmed et al., 2009; Ballard et al., 2016; Bezagu et al., 2015; Ng et al., 2009; Ryu et al., 2004; Wang et al., 2011; Zhou et al., 2015). Mixing efficiency is significantly further improved even within short channel lengths of microfluidic devices and provide controllable mixing, although the overall system can become complicated.

Recently, periodic fluid pulsation methods are utilized to enhance mixing efficiency with several benefits such that they can be easily implemented with microfluidic systems due to the absence of additional requirements (e.g., magnetic particles and electrode patterning) and they effectively increase the degree of mixing in a microscale flow (Abolhasani et al., 2014; Cheng et al., 2018; Kim et al., 2017b; Liu and Rauch, 2003; Phelan Jr et al., 2008). The oscillating input that generates repetitive forward–reverse flow from fluid driving sources (e.g., pneumatic pump and syringe pump) dynamically changes the flow patterns and induce fluid perturbations in microfluidic channels, thereby significantly enhancing the mixing efficiency and it leads to efficient reaction in microfluidic devices. Furthermore, microfluidic reactions based on fluid pulsation methods require significantly lower volumes of sample when compared to those based on conventional passive mixing methods since a certain fixed amount of sample volume repeatedly moves back and forth through the device. The capability to conduct assay with small volumes of sample becomes increasingly important when it is difficult to collect sufficient amounts of sample. For example, only a few microliters of blood are collected from finger pricks.

Thus, in the present study, we present a resettable particle array device that allows the efficient enrichment of molecules of interest on the surface of arrayed microparticles based on affinity-based binding and retrieval of the particles for further off-chip analyses. We combined the advantages of microparticle-incorporating microfluidic platforms and oscillatory flow, and this creates a synergy. Microparticle-incorporating microfluidic assay platforms offer several benefits as follows. (i) When compared to flat substrates, microparticles exhibit high surface-to-volume ratio, and thereby enable rapid analysis, (ii) the surface of microparticles is easily functionalized with a variety of molecule types (e.g., DNA and protein), and (iii) microparticles exhibit the traits of a mobile substrate, and thus allow the enrichment and transport of molecules of interest (Derveaux et al., 2008).

Our device is operated via the following three steps of particle manipulation; (i) particle trapping, (ii) particle securing, and (iii) particle releasing. We exploit the mechanism of structure deformability-based particle handling method reported in our previous study (Kim et al., 2017a), and thus the introduced particles are trapped and subsequently secured inside each array element. The particles remain inside the array element relative to the oscillating flow. In the particle securing step, the target molecules in the surrounding sample liquids are effectively delivered and bound to the particle surfaces under oscillatory flow. The secured particles are released from the array when required, thereby allowing the off-chip collection of microparticles and further analysis. The particle releasing step also allows the device resettability.

We characterized the operation and design parameters of the device and successfully demonstrated particle trapping, securing, oscillating, and releasing. As a proof-of-concept of the method, we performed enhanced molecular binding between an array of streptavidin-conjugated particles and fluorescence-labeled biotin sample, and this is facilitated via increased molecular collision induced by the periodic oscillating sample flow. Furthermore, as a practical application, we performed an on-chip immunoassay to detect anti-Zika nonstructural protein 1 (NS1) monoclonal antibody (mAb) (which is one of the biomarkers for Zika virus (ZIKV) serologic diagnosis) with a sample volume less than 10 μL and a turnaround time of 10 min. From the calibration curve, the limit of detection (LOD) was calculated as approximately 1 ng/mL.

2. Material and methods

2.1. Device design and working principle

The single-layered polydimethylsiloxane (PDMS)-glass hybrid microfluidic device is composed of an inlet to introduce particles and sample liquids, a trapping array (10 columns and 10 rows) to manipulate (i.e., trap, secure, release) particles, and an outlet to collect particles from the device (Fig. 1a). Detail design and dimensions of the device are presented in Fig. S1. We also confirmed that flow distribution is nearly even throughout the trapping array by using COMSOL simulation (Fig. S2). The array element consists of three main components, namely (i) two narrow gaps (i.e., front and rear gap; G_f and G_r), (ii) four deformable membranes for particle trapping, securing, and

releasing under certain flow conditions, and (iii) particle securing room where particles freely move back and forth under the oscillating flow.

We utilized particle handling methods facilitated by elastic membrane deformation as detailed in a previous study (Kim et al., 2017a). The front gap captures the introduced particles, and subsequent particles then bypass the occupied gap (Fig. 1b). Under the increased flow, captured particles pass through the front gap and are re-captured at the rear gap (Fig. 1c). The rear gap is designed as smaller than the front gap to prevent an escape of particles from the array element right after passing through the front gap. It allows the robust retention of microparticles inside the array. Subsequently, secured particles move back and forth inside the array element under the moderate operating flow condition (Fig. 1d). Particles behave as a mobile substrate, and thus various assays can be performed based on the type of functionalized molecules on particle surface (e.g., antibodies, ssDNA) (Conde et al., 2014). The strategy to enhance particle-based mixing efficiency involves exploiting the induced local turbulent flow which is caused by the oscillating motion of microparticles and surrounding sample fluids. The particles are stably secured inside the array, and thus oscillating flow increases the molecular collisions and offers significantly higher binding opportunities between the molecules when compared to diffusion-driven molecular binding in typical microfluidic laminar flows governed by a low Reynolds number. Following the reaction, increased flow releases the particles from the array, and they can be also collected from the outlet for further off-chip analysis (Fig. 1e).

2.2. Device fabrication

The microfluidic device was fabricated with PDMS (Sylgard 184, Dow Corning Inc.) by standard soft lithography (Xia and Whitesides, 1998). In order to prepare a master mold, a photoresist (KMPR1025, MicroChem, Inc.) was patterned onto a 4-in. silicon wafer via UV photolithography. The photoresist was spun onto a silicon wafer with a thickness of 28 μm and baked for 12 min on a 100 °C hot plate. Subsequently, the photoresist pattern was defined by exposing on ultraviolet (UV) through a photomask, and this was followed by post-exposure-baking for 3 min on a 100 °C hot plate and development process via an SU-8 developer (MicroChem, Inc.). PDMS replicas were prepared by using the mold. The PDMS mixture (12:1 w/w ratio of polymer base to curing agent) was poured on the master mold and degassed in a vacuum chamber. The degassed PDMS was thermally cured for 20 min on a 100 °C hot plate and peeled off from the master. The inlet and outlet holes were punched with a disposable biopsy punch and rinsed with isopropanol. The PDMS replica and glass substrate were contacted to seal the microchannel after exposure to ambient air plasma with a plasma system (CUTE-MP, FemtoScience). The bonded microfluidic devices were secured under room temperature for 24 h to ensure reliable sealing.

2.3. Preparation of microparticles

Bare polystyrene particles (average diameter of approximately 20 μm, standard deviation < 0.4 μm, Sigma-Aldrich) and streptavidin-conjugated polystyrene particles (average diameter of approximately 19.1 μm, Spherotech) were purchased and used as is. Suspensions of those particles with desired concentrations were prepared via dilution in deionized water containing 0.5% (v/v) of Tween 20 (Sigma-Aldrich) and 0.1% (w/v) of bovine serum albumin (BSA) (Sigma-Aldrich) to prevent particle aggregates and adhesion of particles to the microchannel. Carboxylated polystyrene particles (average diameter of approximately 20 μm, Kisker Biotech GmbH) were purchased and subsequently treated for the conjugation of ZIKV NS1 that were provided by the Bio Nano Health Guard Research Center (H-GUARD). With respect to the protein conjugation, the 1-ethyl-3-(3-dimethylaminopropyl) carbodiimide (EDC, Thermo-Fisher) and sulfo-N-hydroxysuccinimide (sulfo-NHS, Sigma-Aldrich) method was used. Details of the procedure used for EDC/NHS coupling are given in supplementary information S6.

2.4. Reagents for on-chip immunoreactions

In order to evaluate the immunoreaction efficiency of the proposed method, Atto 550-labeled biotin (Sigma-Aldrich, excitation/emission = 554/576 nm) was used for the streptavidin-biotin interaction as a proof-of-concept. Atto550-labeled biotin solutions (1.5 μM and 13.6 nM) were prepared via dilution in deionized water containing 0.5% (v/v) of Tween 20 and 0.1% (w/v) of BSA. A quantitative on-chip immunoassay was performed for the detection of the anti-Zika NS1 mAb (provided from H-GUARD). Anti-Zika NS1 mAb were prepared with purified recombinant viral NS1 proteins of Zika virus from the baculovirus expression system. Alexa Fluor 546-labeled anti-mouse IgG (invitrogen, excitation/emission = 556/573 nm) were also prepared. In order to prepare a sample solution, different concentrations of anti-Zika NS1 mAb solutions (0, 2, 10, 20, 100, and 200 ng/mL) were mixed with 40 μg/mL Alexa Fluor 546-labeled anti-mouse IgG solution at room temperature for 30 min with gentle shaking. This resulted in sample solutions containing anti-Zika NS1 mAb/Alexa Fluor 546-labeled IgG complex, and the final concentrations of anti-Zika NS1 mAb corresponded to 0, 1, 5, 10, 50, and 100 ng/mL. Dilution was performed with phosphate buffered saline (PBS) (Gibco) containing 0.5% (v/v) of Tween 20. The concentrations of Alexa Fluor 546-labled IgG for the six samples were identical (20 μg/mL).

2.5. Experimental setup

In order to operate the microfluidic device (i.e., trapping, oscillating, and releasing of particles), a custom-built pressure supply system was constructed (Fig. S3). The pressure supply system was composed of a solenoid valve (LHD series, Lee Products, Ltd.), positive and negative pressure pumps, a pressure regulator, a pressure monitor, and a computer. By triggering the solenoid valve with software embedded in PC, the on/off state of solenoid valve was controlled, and it enabled application of either negative or positive pressure to the device for a certain duration. This delivered square-wave-like pressure to the microfluidic device, thereby inducing oscillating flow inside the channel. All microscopic images and videos were obtained by using an inverted microscope (IX 73, Olympus) with a charge coupled device (CCD) camera (DP 80, Olympus). For fluorescence detection, a SOLA light engine (SM 365, lumencor) and filter cube (U-FGWA, Olympus, excitation/emission = 530–550/575–625 nm) were used as the light source and fluorescence filter, respectively. ImageJ software (National Institutes of Health) was used to investigate fluorescence intensities of the microparticles.

3. Results and discussion

3.1. Device characterization

Bare polystyrene microparticles were loaded through the inlet to the trapping array of microfluidic devices by applying a constant pressure difference (i.e., ΔP) of 5 kPa. The trapping array was rapidly saturated with the introduced particles in less than 30 s. The narrow dimension (i.e., narrower than the average particle size) of the front gap allows the capture of only single particles and additional particle trapping was prevented because subsequent particles bypassed the saturated trapping array due to increased hydraulic resistance through the occupied trap sites. In order to investigate trapping efficiencies (i.e., ratio of number of trapped single particles to number of trapping arrays), five devices with different front gap dimensions (corresponding to 16, 17, 18, 19, and 20 μm) were tested (Fig. 2a). The dimensions of the rear gap were designed as equal to the five front gap dimensions (Fig. S1). Trapping efficiencies of > 95% were achieved with the front gaps corresponding to 16, 17, 18, and 19 μm. However, lower trapping efficiency (of

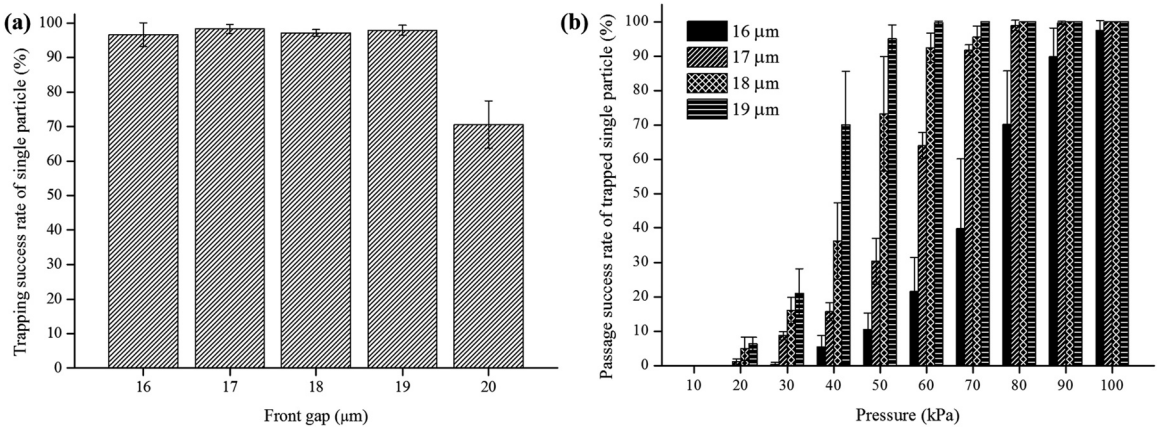

Fig. 2. Device characterization (a) Particle trapping success rate for five different front gap dimensions. With the exception of the 20-μm front gap, trapping efficiencies in the other front gaps (16, 17, 18, and 19 μm) exceeded 95%. (b) Particle passage success rates in the four different front gap dimensions (i.e., gap dimensions that allow a trapping efficiency of > 95%) based on variations in the input pressure value. The results indicate that the narrower gap exhibits lower particle passage success rate at a given input pressure. Thus, critical pressure value tends to increase when the gap dimension decreases. Data are presented as the average ± standard deviation, and all measurements are performed in triplicate.

approximately 70%) was observed when the width of the front gap was 20 μm. In the 20 μm gap device, the trapping failure was caused due to the undesired particle passage (i.e., smaller size particles pass through the gap) given the particle size distribution. Thus, we concluded that the dimension of the front gap should be designed as smaller than the size of the smallest particle to obtain high particle trapping efficiency.

When the trapping array was saturated with the particles, the trapped particles are allowed to pass through the front gap by applying an increased flow rate and subsequently secured inside the trapping array. This enables particle oscillation under periodic oscillating pressure input. The passage of trapped particles was enabled by the deformation of the thin membranes that were in contact with the trapped particles. Membrane deformation was achieved via the increased flow-induced shear stress caused by higher input pressure magnitude (Kim et al., 2017a). We investigated the passage success rate of trapped particles with the four different types of devices with front gaps corresponding to 16, 17, 18, and 19 μm by varying input pressure values (from 10 kPa to 100 kPa with 10 kPa increments) with a fixed input duration of 10 s (Fig. 2b). As expected, under a given input pressure, the particle passage rate tends to decline with decreases in the gap size. In order to determine the device operating input pressure conditions, we set the certain pressure value as a critical pressure value (P_c) that allows almost all (> 95%) the trapped particles to pass through the gap. Critical pressure values were obtained as corresponding to 100, 80, 70, and 50 kPa for the particles passing through the 16, 17, 18, and 19 μm gaps, respectively.

3.2. Particle trapping, securing, and releasing

Based on the device characterization results, we selected a microfluidic device with an array element dimension with a front gap of 19 μm and a rear gap of 16 μm (named as F19R16 device) as the optimum design to conduct particle (average diameter of approximately 20 μm) manipulation. Performance characterization results (i.e., trapping and release success rates) of the F19R16 device are presented in Supplementary information S4. We successfully demonstrated the entire microparticle manipulation steps including trapping, securing, and releasing by using the F19R16 device (Fig. 3). When the particles were trapped at the front gap, redundant particles were washed out, and the trapped particle subsequently passed through the gap when an input pressure value exceeding the critical pressure value of the front gap ($P_{c,front}$ = 50 kPa) was applied. After passing through the front gap, the particles were re-trapped at rear gap because the narrower rear gap exhibits a higher critical pressure value to allow the passage of particles. Thus, the particles stably remained inside the trapping array under both forward and reverse flow conditions when the operating pressure was lower than the critical pressure value of front gap. The particles secured inside the array were released by applying an input pressure value exceeding the critical pressure value of rear gap ($P_{c,rear}$ = 100 kPa), and this provided a simple method to reset the device. Under this pressure condition (i.e., 100 kPa), the particle release efficiency (i.e., ratio of released particles to secured particles inside the array) was close to 100%, thus showing that the device has a potential

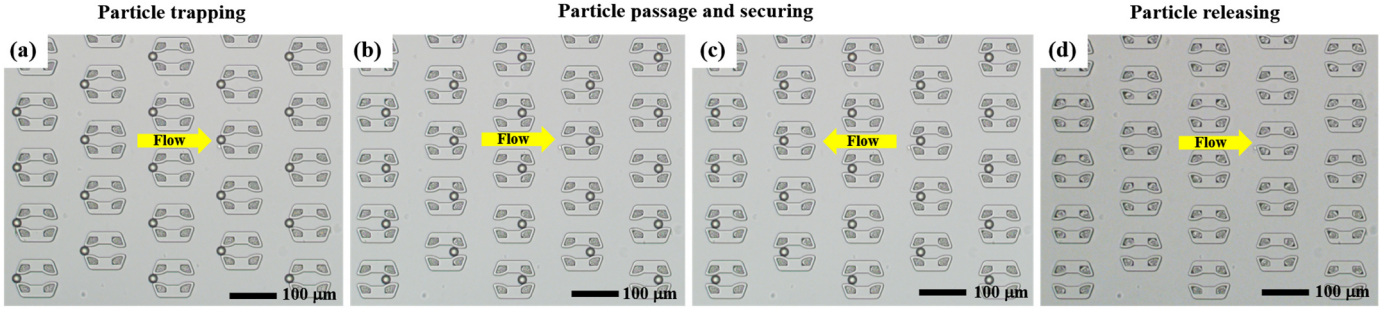

Fig. 3. Device operation. (a) Microscopic image of particle trapping. The trapping array is saturated by single particles, and redundant particles are washed out. (b-c) Particle passage and securing. Trapped particles pass through the front gap via a higher input pressure value to induce sufficient membrane deformation that leads to particle passage. Subsequently, the particles remain inside the particle and secure room under the both forward and reverse flow. In this situation, particle oscillation is performed. (d) Particle releasing. All the secured particles are allowed to escape from the array via the application of higher input pressure in the same manner as the particle passage step.

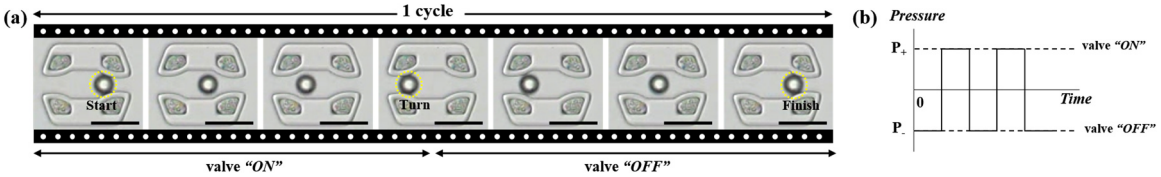

Fig. 4. Oscillation motion of secured particle. (a) Sequential images of particle oscillation under the periodic square-wave pressure input. "Start-turn-finish" of particle movement is defined as 1 cycle. The images are obtained from the experimental condition of solenoid valve switching time corresponding to 200 ms and input pressure values corresponding to + 1 and − 1 kPa, respectively. Under the condition, the period for 1 cycle is 0.4 s. Scale bars: 50 μm. (b) Illustration of square-wave pressure input to induce particle oscillating motion resulting from the negative and positive pressure sources and the on/off switching control of the solenoid valve.

resettable capability. Additionally, the released particles can be collected at the outlet and used for further off-chip analyses.

3.3. Oscillation of particles

Periodical back and forth motion (i.e., oscillation) of microparticles and surrounding liquids was performed by generating square-wave shaped pneumatic pressure profile at the outlet of the device by using the pressure supply system (Fig. 4). When the state of solenoid valve corresponded to "on", particles move towards the inlet of the device via the positive pressure input. Conversely, particles moved back to their initial position when the solenoid valve corresponded to the "off" state. Various profiles of oscillation motion are achieved via regulating the input pressure values and solenoid valve switching time. Oscillatory movement of particles is presented in Video S1.

3.4. Enhancement of particle-based immunoreaction efficiency under oscillatory flow

As a proof-of-concept of our method, we evaluated the immunoreaction efficiencies by using the affinity-based specific binding between streptavidin-conjugated microparticles and Atto550-labeled biotin solutions by varying flow conditions (Fig. 5a). In order to prevent non-specific protein binding on the channel surface, the microfluidic device was pre-filled with deionized water containing 0.5% (v/v) of Tween 20 and 0.1% (w/v) of BSA prior to loading the particles. The particles were robustly secured in the array via the method described above and were subsequently stained by surrounding solutions. Given the high binding affinity between streptavidin and biotin, fluorescence signal intensity of particle increased following the occurrence of the molecular binding events with time. We measured the fluorescence signals from the particle array and analyzed the same to evaluate immunoreaction efficiency.

First, we measured fluorescence signals of particles under static and oscillatory flow conditions by preparing 10 μL volume of 1.5 μM Atto550-biotin sample solution. When the flow was stationary, a distinct signal increase was not observed over time, and this was due to low molecular collision and binding chance. Conversely, oscillatory flow-assisted immunoreaction method exhibited a gradually increasing signal, thereby demonstrating efficient molecular binding performance with respect to the limited volume of sample liquids. Sample consumption was measured as approximately 7.3 μL under the experimental condition corresponding to $\Delta P = 10$ kPa and a period of 1 cycle = 8 s to conduct a 10-min experiment. The oscillatory flow consumes a certain fixed volume irrespective of the reaction time since a certain fixed volume of sample repeatedly moves back and forth through the device and facilitates an efficient immunoreaction with limited amount of sample (Fig. 5b). A schematic of the oscillating flow of sample liquid through the device is presented in Fig. S4.

This is followed by a comparison to evaluate the efficiency of

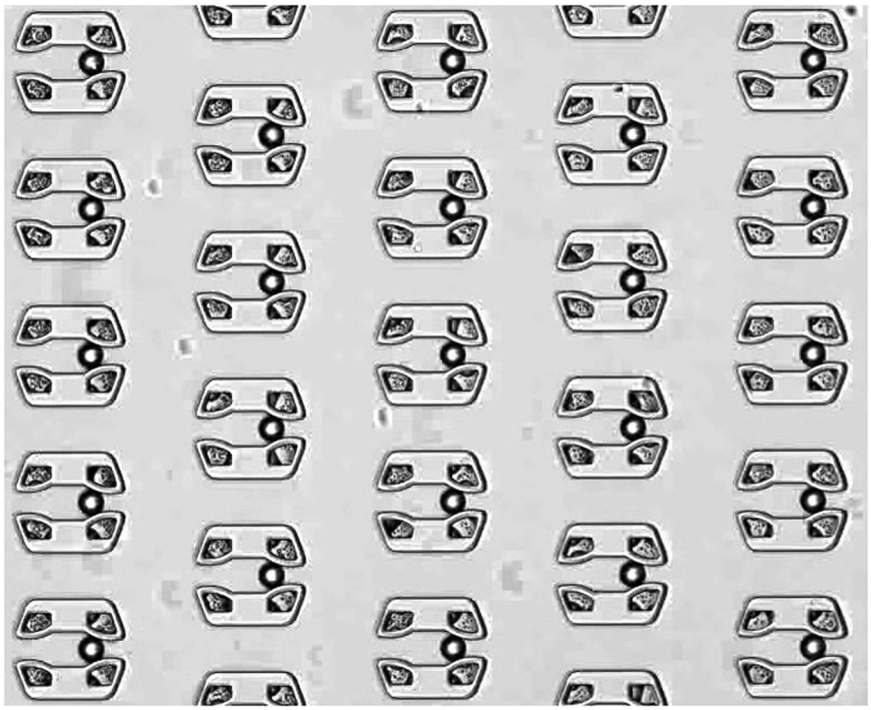

Video S1. Oscillatory movement of particles. Supplementary material related to this article can be found online at: doi:10.1016/j.bios.2019.01.067.

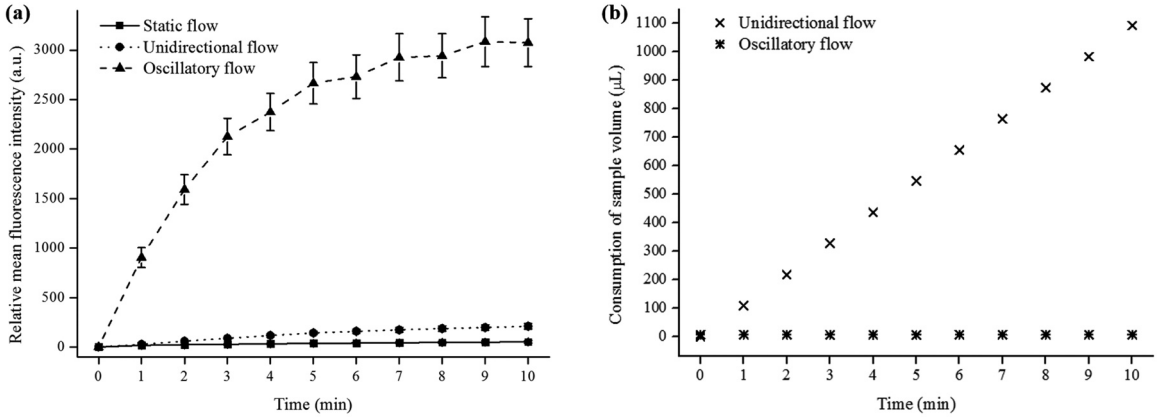

Fig. 5. Microparticle-incorporating on-chip immunostaining results. (a) Average fluorescence intensities of streptavidin-conjugated particles over time under static, unidirectional, and oscillatory flow of Atto550-biotin solution. A distinct signal change is not observed in the static condition. A slight signal increase is observed in the unidirectional flow condition. Oscillatory flow condition facilitates efficient molecular binding with limited volume of sample liquids. (b) Consumption of sample volumes under unidirectional and oscillatory flow. Oscillatory flow consumes a fixed amount of volume irrespective of reaction time. Consumption of the sample volume of unidirectional flow-based assay increases with increases in the reaction time.

unidirectional flow-based immunoreaction (i.e., continuous fluid flow from inlet to outlet) wherein we prepared a sample solution by diluting 10 μL of 1.5 μM of Atto550-biotin sample solution with 1090 μL of deionized water containing 0.1% (w/v) BSA and 0.5% (v/v) Tween 20 to result in 1.1 mL of 13.6 nM Atto550-biotin solution. We diluted the sample because the required sample volume was measured as approximately 1.1 mL to perform a 10-min experiment under the unidirectional flow condition in the pressure condition corresponding to ΔP = 10 kPa. As shown in Fig. 5a, fluorescence signal increased slightly over time. The results indicate the advantages of oscillatory flow-based immunoreaction in terms of its capability to perform an efficient reaction with limited amounts of the sample.

3.5. Detection of anti-Zika NS1 monoclonal antibody

Rapid spread of mosquito-borne ZIKV was first reported in May 2015 in Brazil and aroused global attention since ZIKV infection causes newborn microcephaly and serious neurological complications (Petersen et al., 2016). Thus, in order to demonstrate the applicability of our method, we performed an immunoassay to quantitatively detect biomarkers for ZIKV serologic diagnosis (i.e., anti-Zika NS1 antibody) by using the method presented in the study. A common protocol for conventional immunoassay corresponds to the enzyme-linked immunosorbent assay (ELISA). However, it typically consumes large amount of samples and is time-consuming and labor-intensive. The method proposed in the study facilitates an efficient immunoassay with a limited sample volume (< 10 μL) and short assay time (approximately 10 min). Specifically, PBS containing 0.5% (v/v) of Tween 20 and 0.1% (w/v) of BSA was filled in a microchannel to prevent non-specific protein binding prior to the test. Additionally, ZIKV NS1-conjugated polystyrene particles were loaded to construct an array of secured particles. A calibration curve was obtained for the assay by using an array of the particles conjugated with ZIKV NS1 and a sample solution containing various concentrations of anti-Zika NS1 mAb coupled with a fluorescence-labeled anti-mouse IgG (Fig. 6). Five concentrations of sample solution were prepared in the range of 1–100 ng/mL. After completing 10-min of multiple cycles of oscillation (ΔP = 10 kPa and period of 1 cycle = 8 s) and washing the microchannel with PBS containing 0.5% (v/v) of Tween 20 and 0.1% (w/v) of BSA to remove any unbound analytes, fluorescence signals from the particles were obtained and investigated. The limit of detection (LOD) can be as low as approximately 1 ng/mL for the detection of anti-Zika NS1 mAb, and this was calculated by adding thrice the standard deviations to the average value of the control sample (i.e., 0-ng/mL sample). Analytical performances of this method, including limit of detection (LOD), limit of quantification (LOQ), precision, and accuracy, are provided in supplementary information S7.

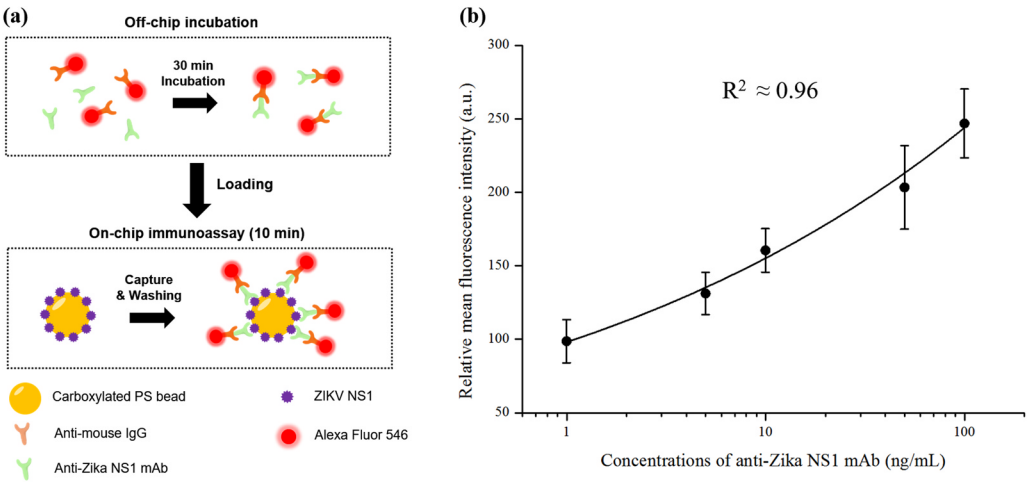

Fig. 6. Oscillatory flow-assisted on-chip quantitative immunoassay for detection of anti-Zika NS1 mAb. (a) Schematic illustration of the detection of anti-Zika NS1 mAb. (b) Assay is performed by using five samples spiked with various concentrations of anti-Zika NS1 mAb ranging from 1 to 100 ng/mL. Fluorescence intensities from an array of particles are measured after sample oscillation and washing non-specifically bound analytes. Limit of detection (LOD) is calculated as approximately 1 ng/mL. Data for the 0-ng/mL sample is not plotted in the graph. Data are presented as the average ± standard deviation. R^2 value is obtained via a four-parameter logistic fit (4-PL fit) and approximately 0.96.

4. Conclusion

In the study, we demonstrated the oscillatory flow-assisted efficient target enrichment method with low sample volume consumption by using particle-based resettable microarray device. By utilizing the flow-induced elastic membrane deformation, particle manipulation was successfully performed with a multi-step process as follows: trapping, passage and securing, oscillating, and releasing. When the particles were robustly secured inside the array, oscillation of particles and surrounding sample liquids was facilitated via the application of square-wave-like input pressure. By using streptavidin-conjugated microparticles and fluorophore-labeled biotin samples, we showed that oscillatory-flow assisted immunoreaction was significantly more efficient when compared to stationary or unidirectional sample flow conditions. Oscillatory flow enabled efficient target molecule enrichment on the surface of particles with limited sample volume ($< 10\,\mu L$) by increasing molecular collision chance. The applicability of the method was investigated by detecting anti-Zika NS1 mAb with LOD of approximately 1 ng/mL with 10-min on-chip immunoreaction. The method presented in the study exhibits advantages including small sample consumption, easy operation, efficient immunoreaction, and the possibility of particle-mediated transport of enriched molecules. However, the limitations of this method are that multiplex immunoassay and selective extraction of particles of interest cannot be achieved. For a future study, these limitations should be addressed by integrating active microvalve structures (e.g., pneumatic pressure-based microvalves) and encoded microparticles. This will enable our method to be used as an efficient tool to conduct multiplex immunoassays and further off-chip analyses by constructing an array of different types of surface-functionalized microparticles that are individually identifiable through encoding/decoding strategy and selective extraction of particles.

CRediT authorship contribution statement

Sanghyun Lee: Conceptualization, Methodology, Investigation, Writing - original draft, Writing - review & editing. **Wonhyung Lee:** Validation, Investigation, Formal analysis, Resources, Visualization. **Hojin Kim:** Conceptualization, Methodology. **Pan Kee Bae:** Resources, Validation. **Jaechan Park:** Resources. **Joonwon Kim:** Supervision.

Acknowledgements

This research was supported by Basic Science Research Program through the National Research Foundation of Korea (NRF) funded by the Ministry of Science and ICT (No. NRF-2017R1A2B4003328) and a grant of the Korea Health Technology R&D Project through the Korea Health Industry Development Institute (KHIDI), funded by the Ministry of Health & Welfare, Republic of Korea (Grant No. HI15C0001).

Declaration of interests

None.

Appendix A. Supporting information

Supplementary data associated with this article can be found in the online version at doi:10.1016/j.bios.2019.01.067.

References

Abolhasani, M., Oskooei, A., Klinkova, A., Kumacheva, E., Günther, A., 2014. Lab Chip 14 (13), 2309–2318.
Ahmed, D., Mao, X., Juluri, B.K., Huang, T.J., 2009. Microfluid. Nanofluid. 7 (5), 727.
Ballard, M., Owen, D., Mills, Z.G., Hesketh, P.J., Alexeev, A., 2016. Microfluid. Nanofluid. 20 (6), 88.
Bezagu, M., Arseniyadis, S., Cossy, J., Couture, O., Tanter, M., Monti, F., Tabeling, P., 2015. Lab Chip 15 (9), 2025–2029.
Cheng, D., Yu, Y., Han, C., Cao, M., Yang, G., Liu, J., Chen, X., Peng, Z., 2018. Biomicrofluidics 12 (3), 034105.
Conde, J., Dias, J.T., Grazú, V., Moros, M., Baptista, P.V., de la Fuente, J.M., 2014. Front. Chem. 2, 48.
Derveaux, S., Stubbe, B., Braeckmans, K., Roelant, C., Sato, K., Demeester, J., De Smedt, S., 2008. Anal. Bioanal. Chem. 391 (7), 2453.
Hong, C.-C., Choi, J.-W., Ahn, C.H., 2004. Lab Chip 4 (2), 109–113.
Kim, D.S., Lee, S.H., Kwon, T.H., Ahn, C.H., 2005. Lab Chip 5 (7), 739–747.
Kim, H., Lee, S., Lee, W., Kim, J., 2017a. Adv. Mater. 29 (31).
Kim, S., Kwon, S., Cho, C.H., Park, J.-K., 2017b. Lab Chip 17 (4), 702–709.
Kwak, T.J., Nam, Y.G., Najera, M.A., Lee, S.W., Strickler, J.R., Chang, W.-J., 2016. PLoS One 11 (11), e0166068.
Li, Y., Liu, C., Feng, X., Xu, Y., Liu, B.-F., 2014. Anal. Chem. 86 (9), 4333–4339.
Lin, D., He, F., Liao, Y., Lin, J., Liu, C., Song, J., Cheng, Y., 2013. J. Opt. 15 (2), 025601.
Liu, Y., Rauch, C.B., 2003. Anal. Biochem. 317 (1), 76–84.
Ng, W.Y., Goh, S., Lam, Y.C., Yang, C., Rodríguez, I., 2009. Lab Chip 9 (6), 802–809.
Petersen, E., Wilson, M.E., Touch, S., McCloskey, B., Mwaba, P., Bates, M., Dar, O., Mattes, F., Kidd, M., Ippolito, G., 2016. Int. J. Infect. Dis. 44, 11–15.
Phelan Jr, F.R., Hughes, N.R., Pathak, J.A., 2008. Phys. Fluids 20 (2), 023101.
Ryu, K.S., Shaikh, K., Goluch, E., Fan, Z., Liu, C., 2004. Lab Chip 4 (6), 608–613.
Suh, Y.K., Kang, S., 2010. Micromachines 1 (3), 82–111.
Therriault, D., White, S.R., Lewis, J.A., 2003. Nat. Mater. 2 (4), 265.
Wang, X., Chen, X., Ma, X., Kong, X., Xu, Z., Wang, J., 2011. Talanta 84 (2), 565–571.
Ward, K., Fan, Z.H., 2015. J. Micromech. Microeng. 25 (9), 094001.
Xia, Y., Whitesides, G.M., 1998. Angew. Chem. Int. Ed. 37 (5), 550–575.
Zhou, B., Xu, W., Syed, A.A., Chau, Y., Chen, L., Chew, B., Yassine, O., Wu, X., Gao, Y., Zhang, J., 2015. Lab Chip 15 (9), 2125–2132.